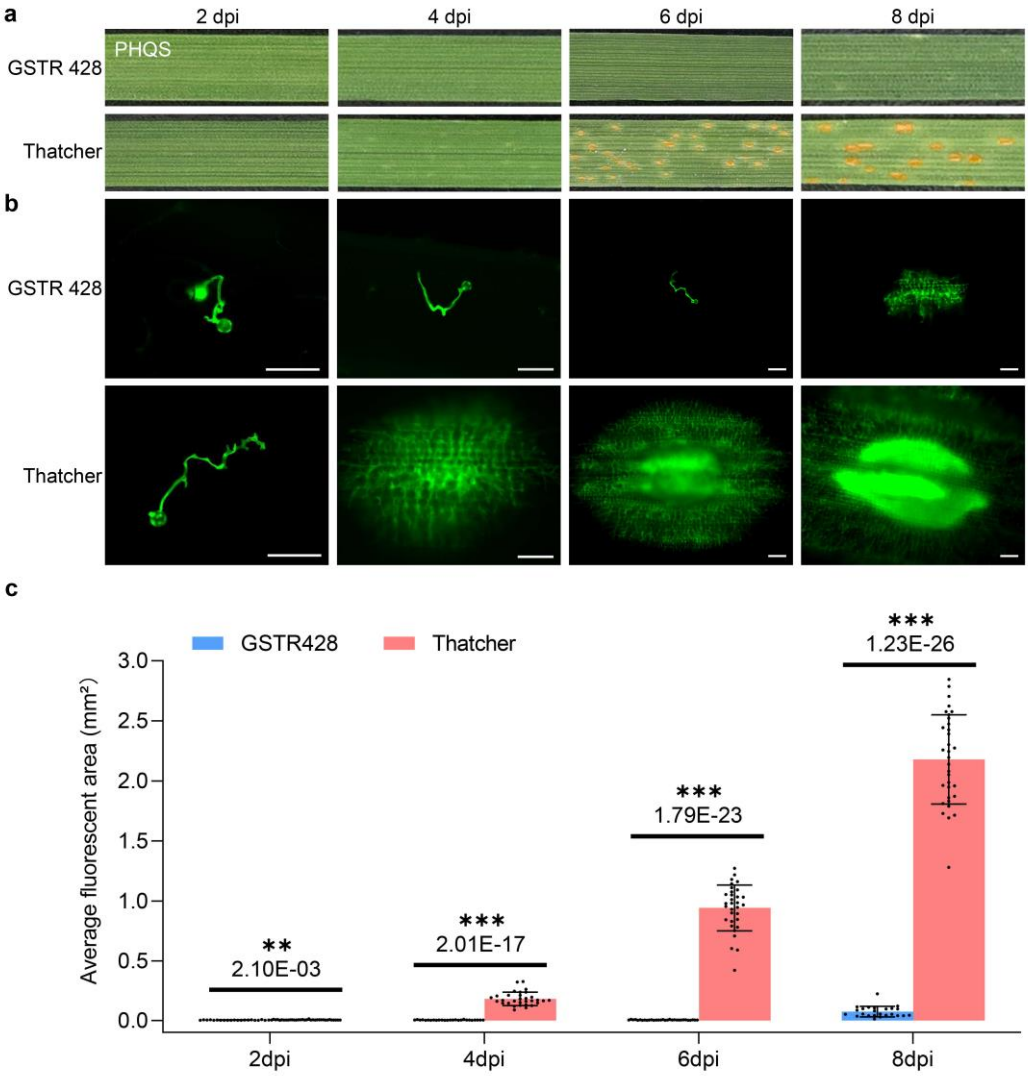
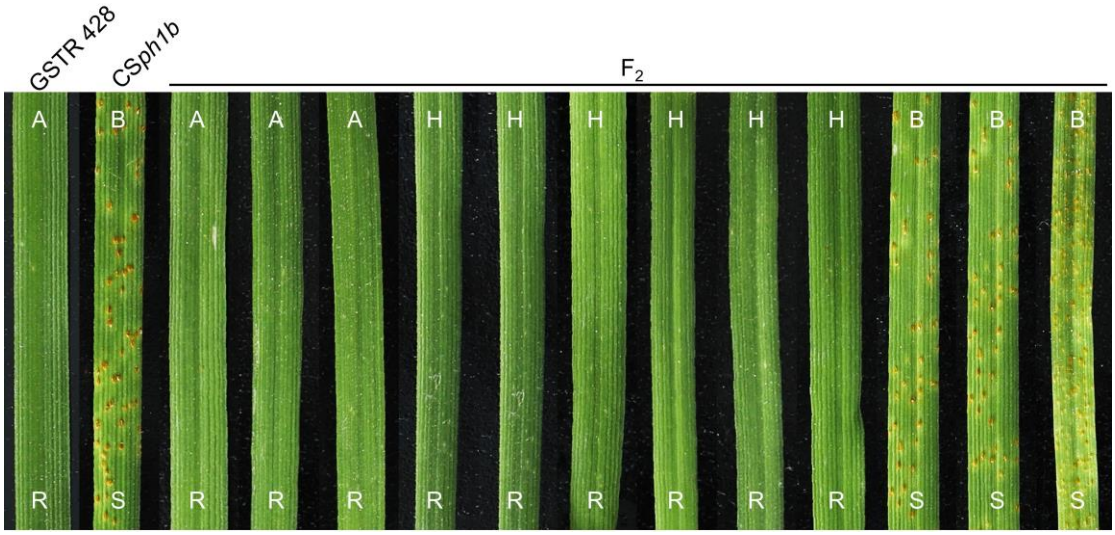
The wheat *Lr28* locus harbors three tandem NLR genes that independently confer leaf rust resistance

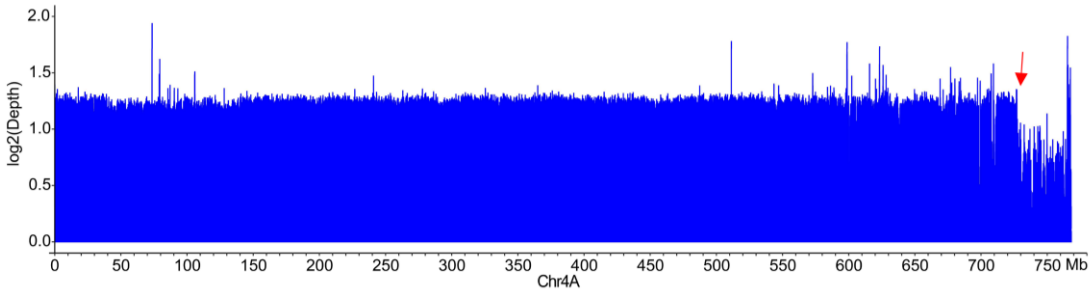
Qiao *et al*.



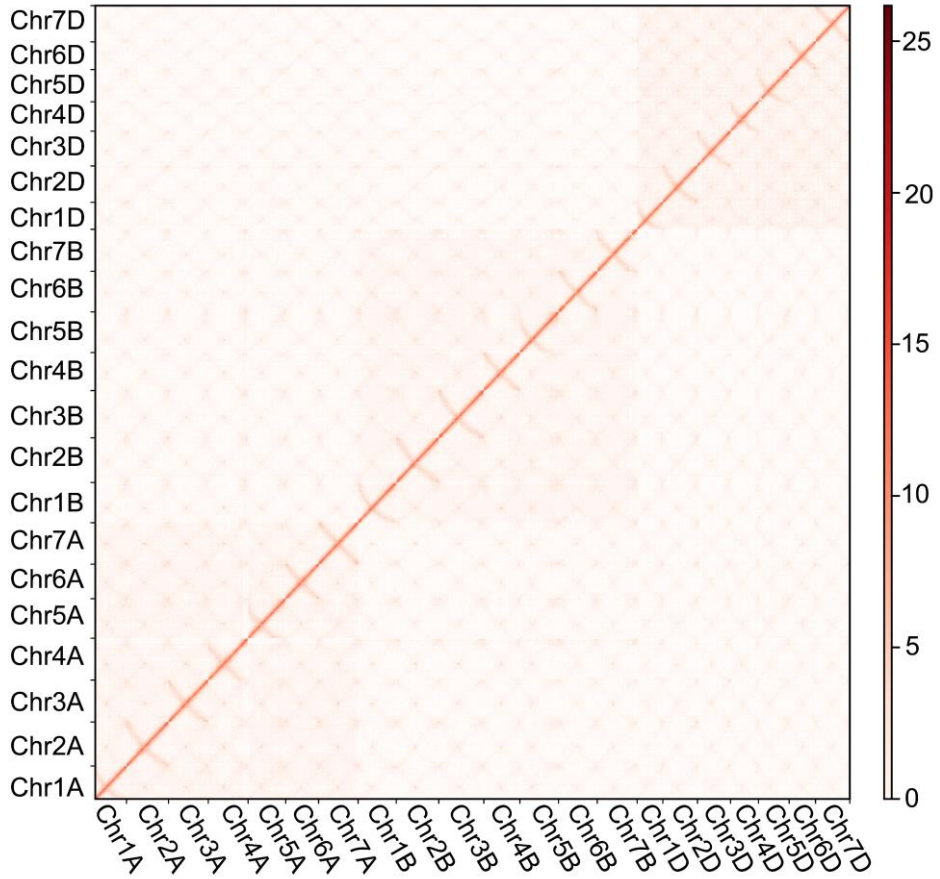
Supplementary Fig. 1. Infection responses of GSTR 428 and Thatcher to *Pt* pathotype PHQS. a, Disease phenotypes at 2, 4, 6, and 8 dpi. **b**, Fluorescence micrographs of fungal hyphae stained with WGA-FITC. Scale bars represent 100 µm. **c**, Quantification of average infection areas in GSTR 428 (blue) and Thatcher (red) at 2-8 dpi. Data were derived from at least 20 independent infection sites per line per time point ($n \geq 20$); individual data points are shown as black dots. Error bars represent standard errors of the means (SEM). Asterisks indicate the level of significance by two-sided unpaired *t*-test. ***$P < 0.001$ and **$P < 0.01$. Source data are provided as a Source Data file.



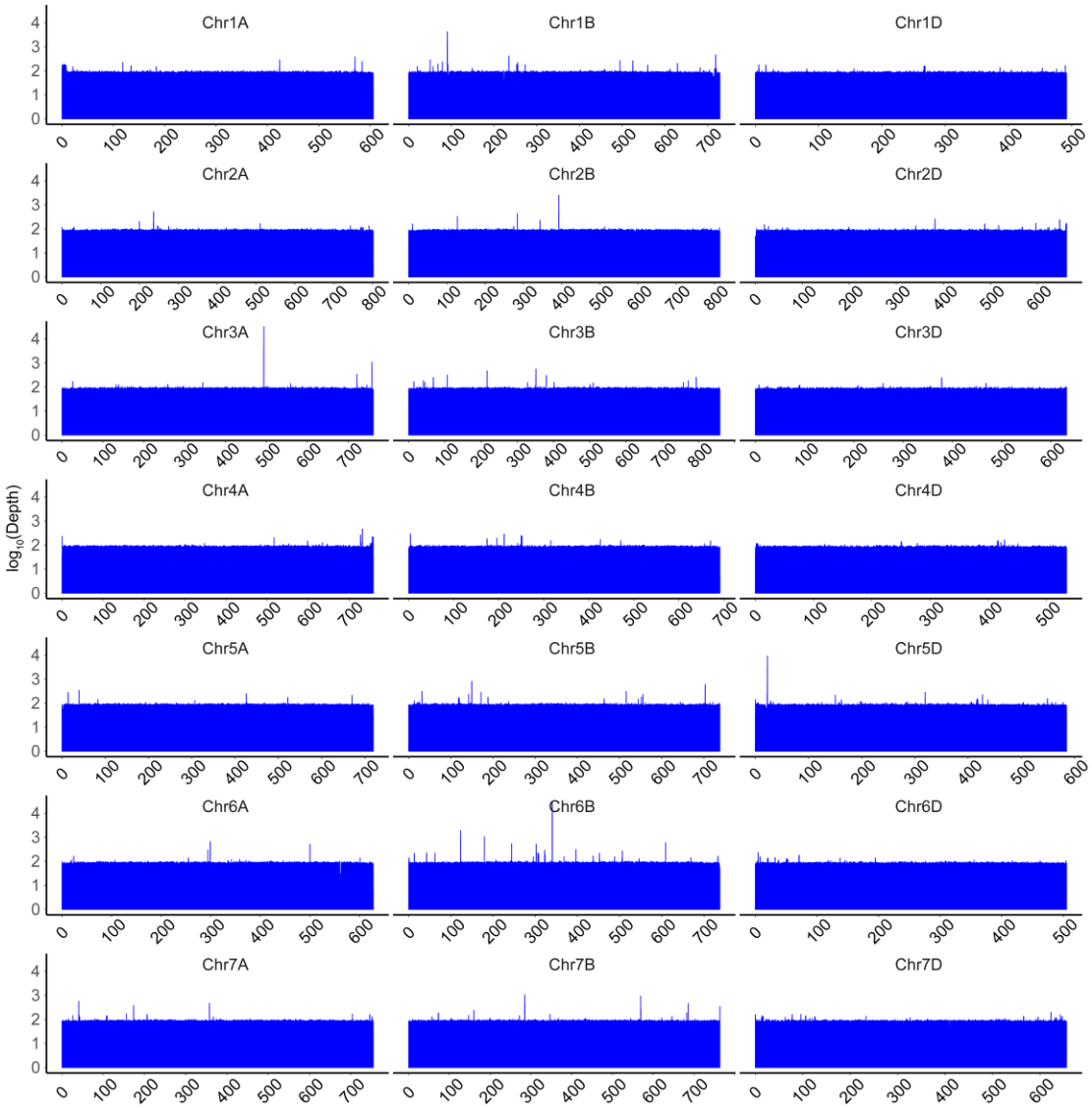
Supplementary Fig. 2. Disease infection phenotypes of F_2 plants derived from the GSTR 428 × CS*ph1b* cross in response to *Pt* pathotype PHQS. A, plants homozygous for the GSTR 428 allele; B, plants homozygous for the CS*ph1b* allele; H, heterozygous. R, resistant; S, susceptible.



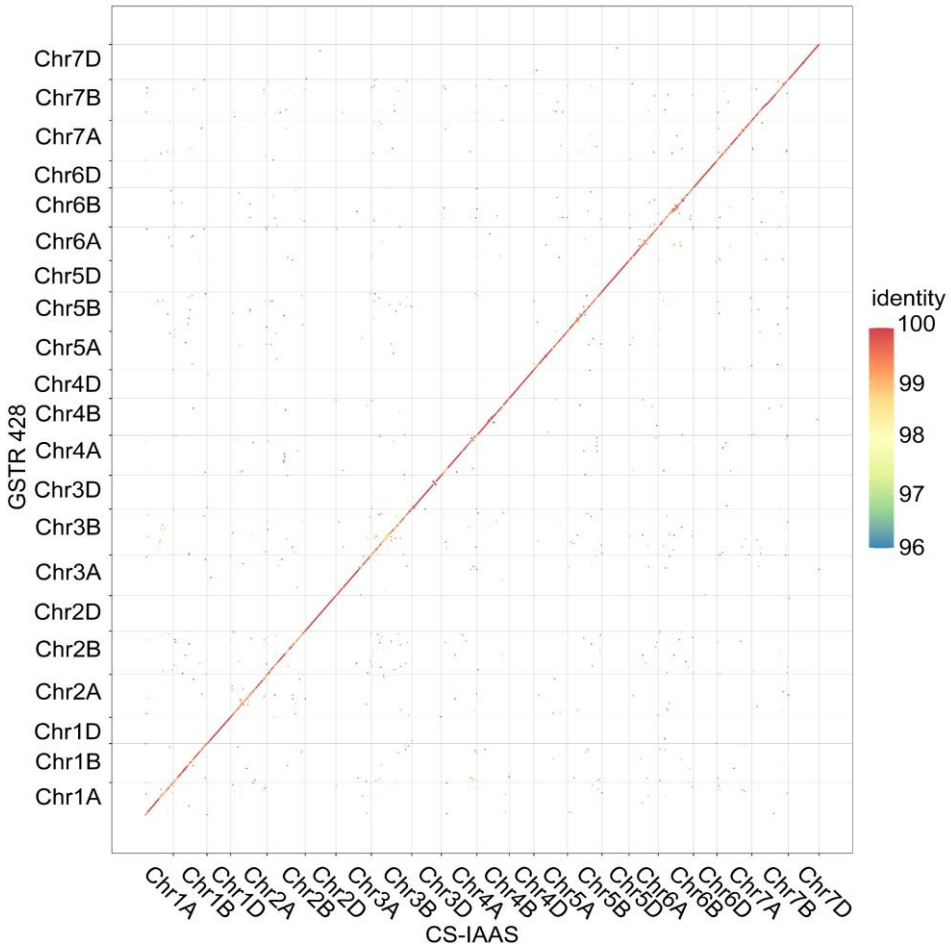
Supplementary Fig. 3. Depth distribution of GSTR 428 whole-genome resequencing reads mapped to the CS-IAAS reference genome. Regions with significantly reduced depth indicate potential alien introgressions. The x-axis represents chromosomal position (in Mb), and the y-axis indicates sequencing depth. The red arrow indicates the position at ~726.90 Mb (based on the CS-IAAS coordinates).



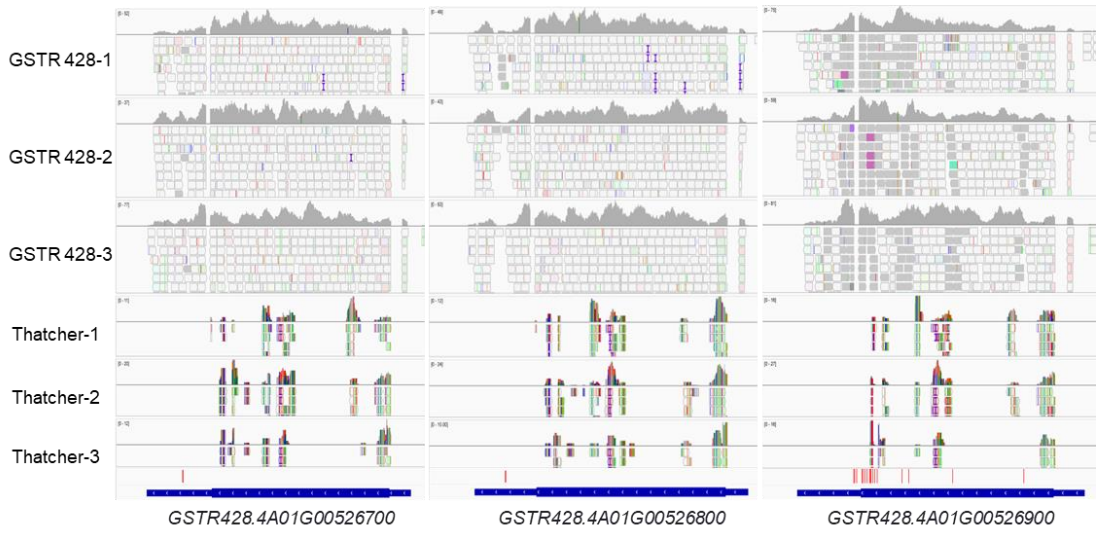
Supplementary Fig. 4. Genome wide Hi-C interaction heatmap for all 21 chromosomes of GSTR 428. The clear diagonal blocks relative to inter chromosomal regions validate the chromosome scale assembly and correct scaffold ordering.



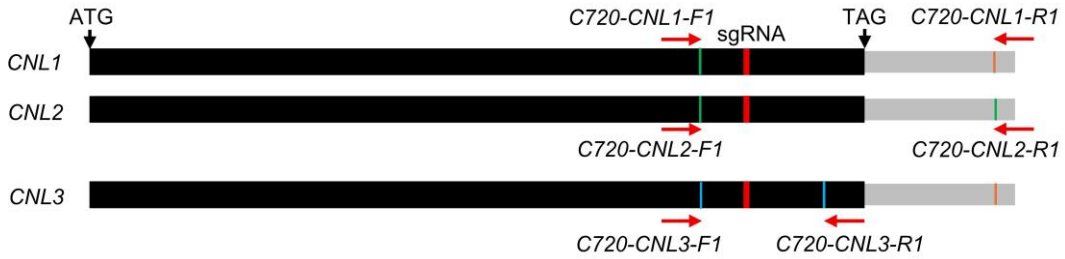
Supplementary Fig. 5. Depth distribution of HiFi reads re-mapped to the GSTR 428 genome assembly. The x-axis represents chromosomal position (in Mb), and the y-axis indicates sequencing depth.



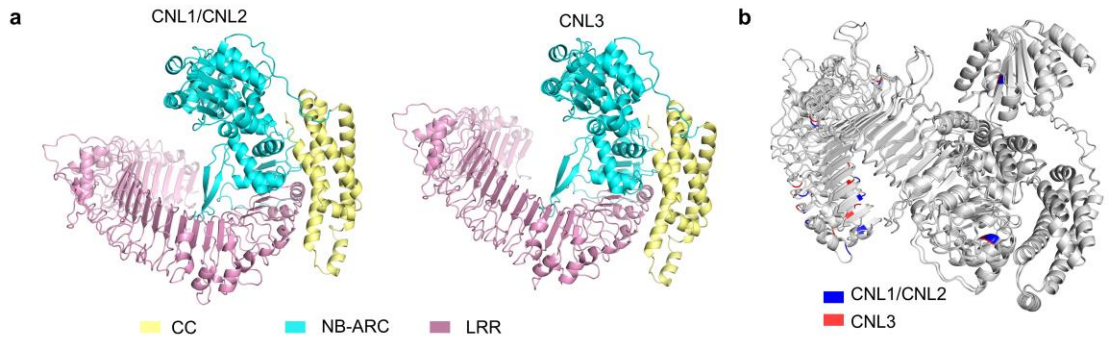
Supplementary Fig. 6. Whole-genome dot-plot comparison between GSTR 428 (y-axis) and the CS-IAAS reference genome (x-axis). Each dot represents a collinear block with 96-100% nucleotide identity.



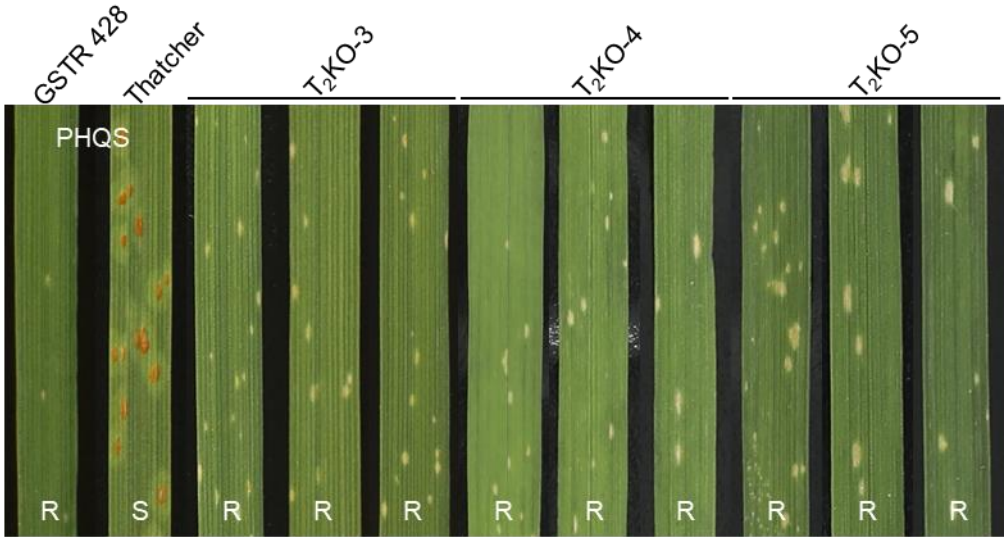
Supplementary Fig. 7. IGV snapshots showing RNA-seq read alignments to the *Lr28* candidate genes. RNA-seq data from GSTR 428 and Thatcher at 72 hpi with PHQS were used. Coverage tracks indicate alignment depth at each nucleotide position. In the alignment panels, gray reads represent uniquely mapped reads and white reads denote multi-mapping reads. Red vertical lines at the bottom of the alignment panels indicate gene specific polymorphisms.



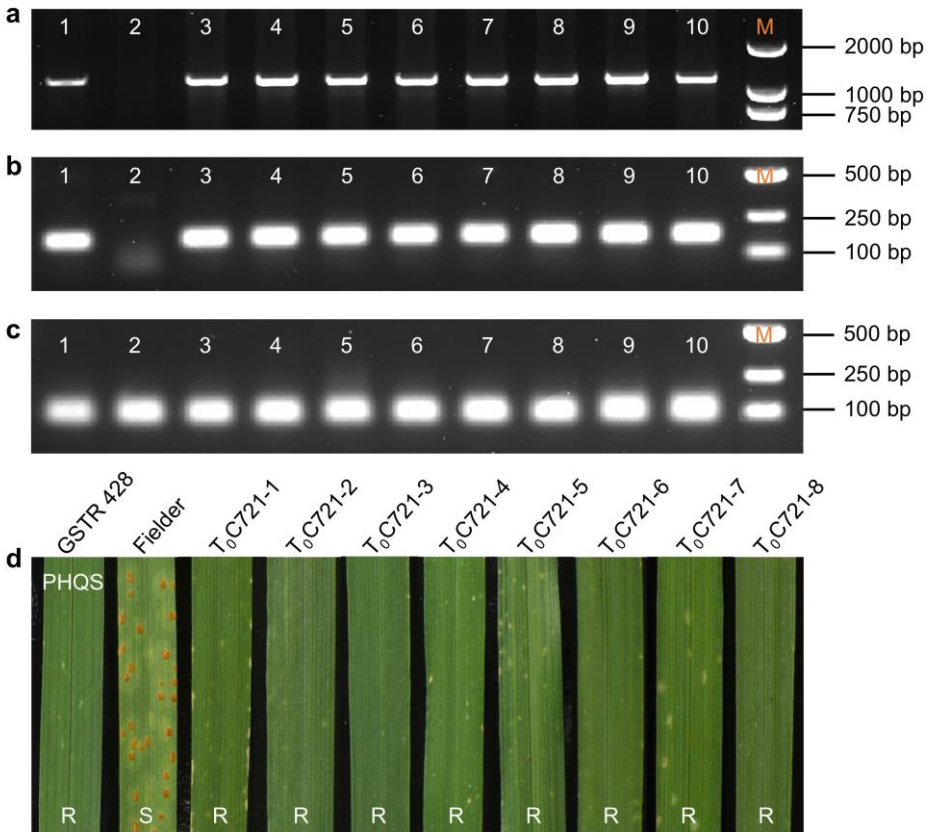
Supplementary Fig. 8. Gene-specific markers for distinguishing *CNL1*, *CNL2*, and *CNL3*. Primer pairs *C720-CNL1-F1R1*, *C720-CNL2-F1R1*, and *C720-CNL3-F1R1* are listed in Supplementary Table 5. Both forward and reverse primers (indicated by red arrows) were designed based on unique polymorphisms located in the coding or downstream regions. Black and gray bars represent coding sequences and the region downstream of the stop codon (TAG), respectively. The single guide RNA (sgRNA) target sites are marked by red rectangles, and sequence polymorphisms are highlighted with colored lines.



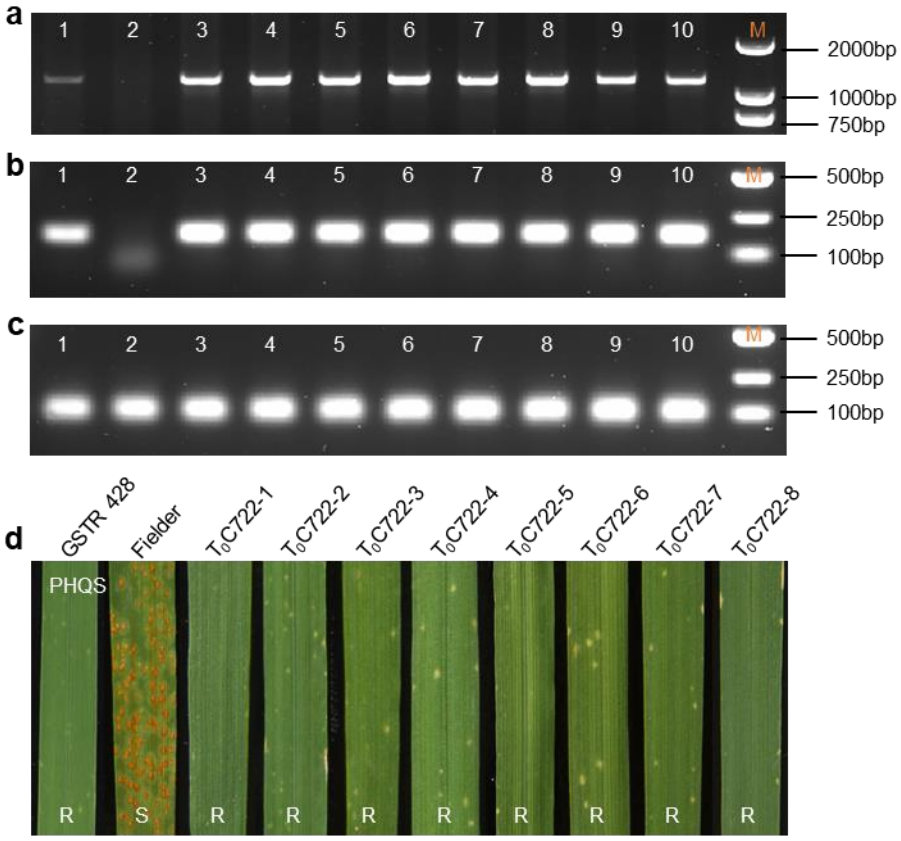
Supplementary Fig. 9. AlphaFold-predicted structural models of CNL1/CNL2 and CNL3. a, Domain-colored models of CNL1/CNL2 (left) and CNL3 (right). The CC domain is shown in yellow, the NB-ARC domain in cyan, and the LRR domain in pink. **b**, Superimposed structures of CNL1/CNL2 and CNL3. Blue and red spheres mark variant residues between the two proteins (blue for CNL1/CNL2 residues; red for CNL3 residues).



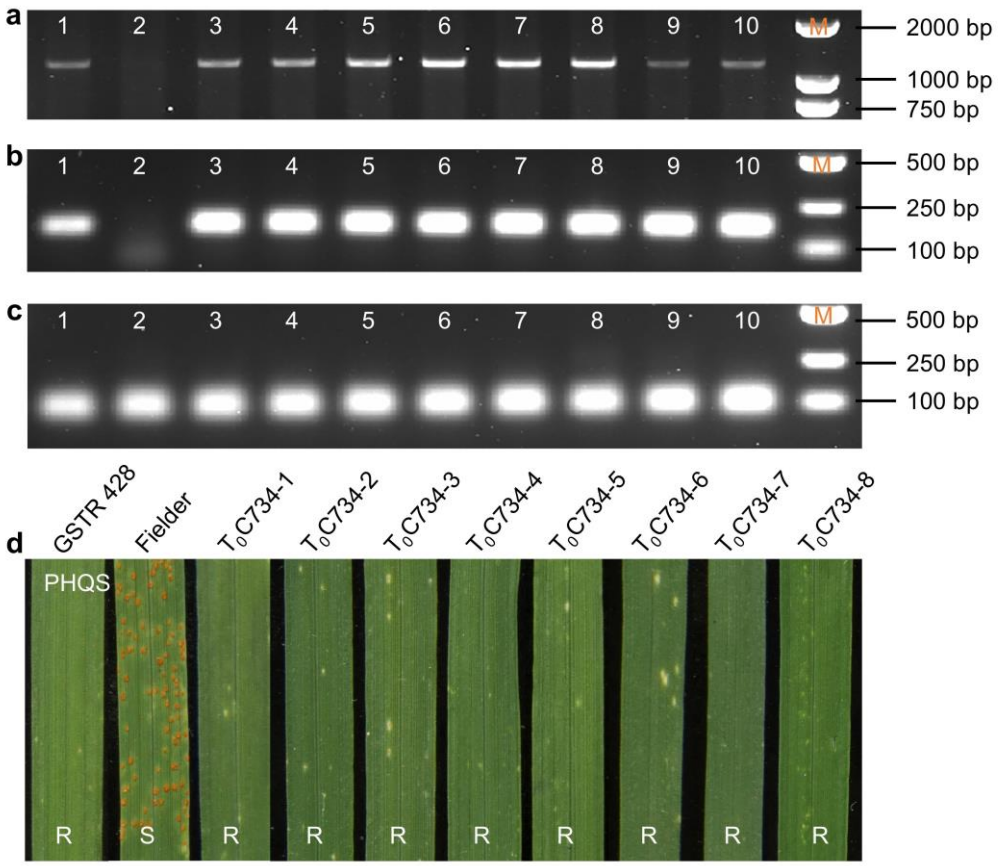
Supplementary Fig. 10. Infection phenotypes of GSTR 428, Thatcher, and transgenic T_2 plants from the T_2KO-3, T_2KO-4, and T_2KO-5 families in response to *Pt* pathotype PHQS. T_2KO-3 carries only *CNL1*; T_2KO-4 carries only *CNL2*; and T_2KO-5 carries only *CNL3*. Their genotypes were confirmed by Sanger sequencing. R, resistant; S, susceptible.



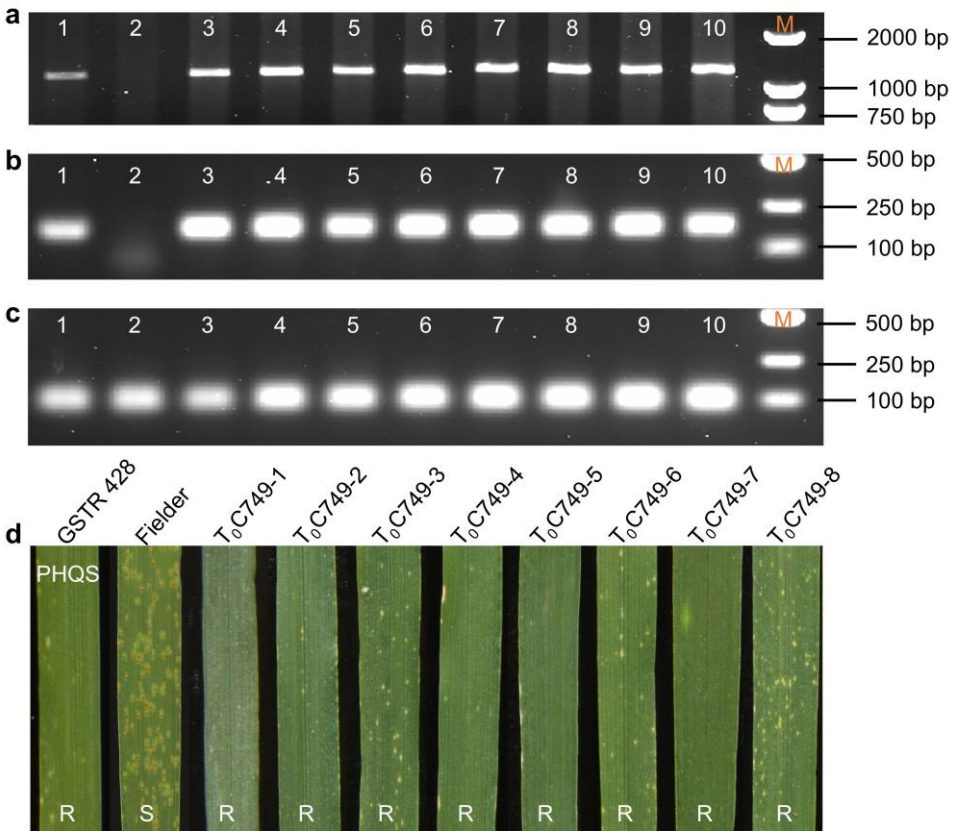
Supplementary Fig. 11. Characterization of T_0C721 (*CNL1*/*CNL2*) overexpression transgenic plants. a, PCR detection of the *CNL1*/*CNL2* transgene (CDS) using marker *Lr28F2R2* in T_0 transgenic plants. **b**, qRT-PCR analysis of *CNL1*/*CNL2* expression. **c**, qRT-PCR amplification of *Actin* as an endogenous control. **d**, Disease reactions of GSTR 428, Fielder, and eight randomly selected T_0 transgenic plants following inoculation with *Pt* pathotype PHQS. R, resistant; S, susceptible. Lane designations: M, DNA marker; 1, GSTR 428; 2, Fielder; 3-10, T_0C721-1 to T_0C721-8, respectively.



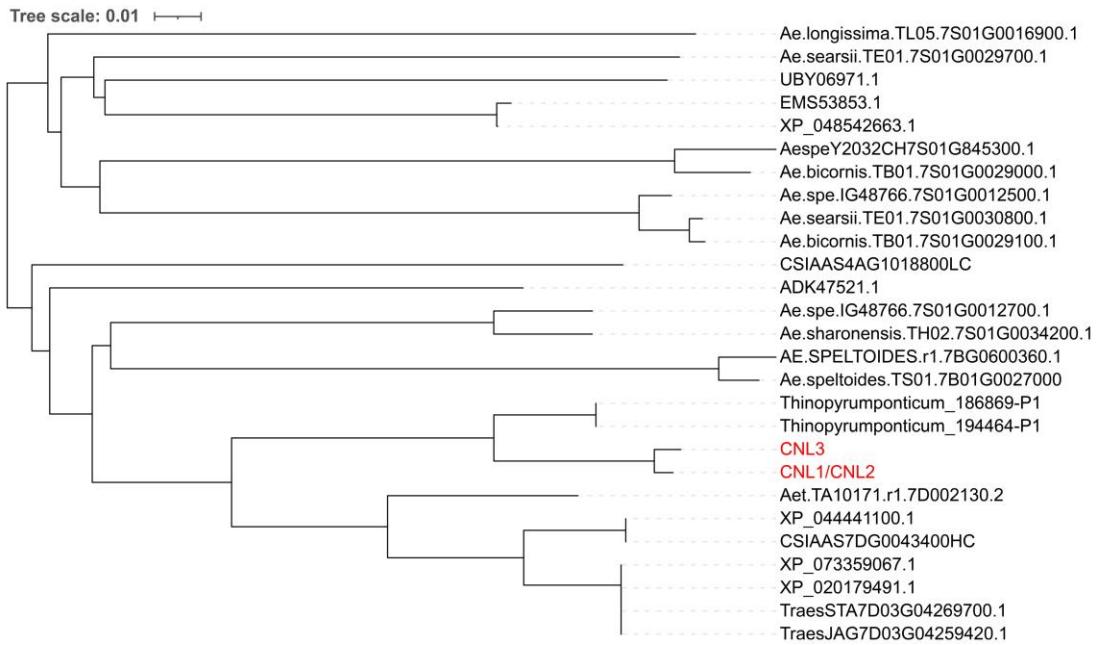
Supplementary Fig. 12. Characterization of T_0C722 (*CNL3*) overexpression transgenic plants. a, PCR detection of the *CNL3* transgene (CDS) using marker *Lr28F2R2* in T_0 transgenic plants. **b**, qRT-PCR analysis of *CNL3* expression. **c**, qRT-PCR amplification of *Actin* as an endogenous control. **d**, Disease reactions of GSTR 428, Fielder, and eight randomly selected T_0 transgenic plants following inoculation with *Pt* pathotype PHQS. R, resistant; S, susceptible. Lane designations: M, DNA marker; 1, GSTR 428; 2, Fielder; 3-10, T_0C722-1 to T_0C722-8, respectively.



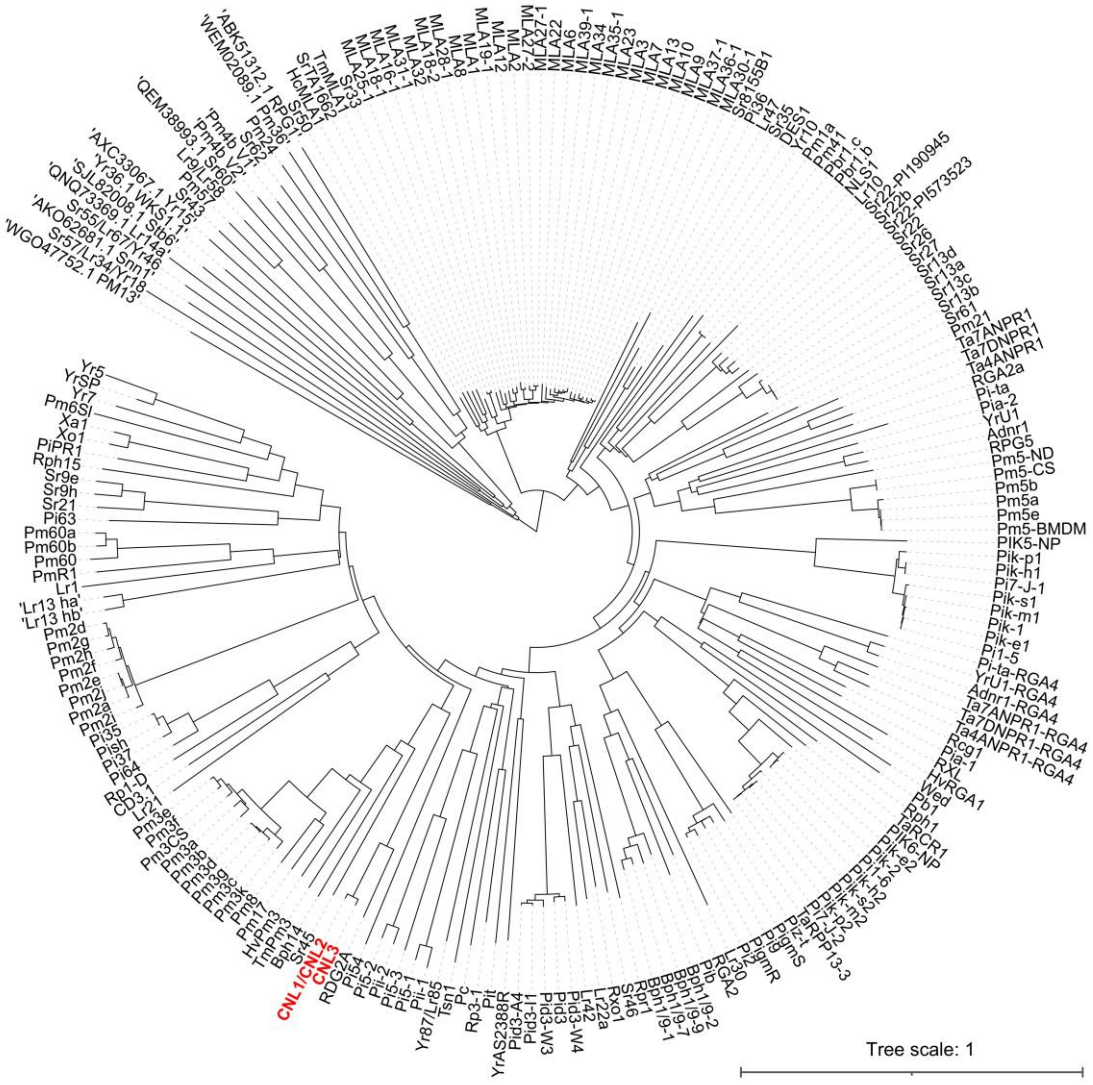
Supplementary Fig. 13. Characterization of T_0C734 (*CNL1*) transgenic complementation plants. a, PCR detection of the *CNL1* (gDNA) transgene using marker *Lr28F2R2* in T_0 transgenic plants. **b**, qRT-PCR analysis of *CNL1* expression. **c**, qRT-PCR amplification of *Actin* as an endogenous control. **d**, Disease reactions of GSTR 428, Fielder, and eight randomly selected T_0 transgenic plants following inoculation with *Pt* pathotype PHQS. R, resistant; S, susceptible. Lane designations: M, DNA marker; 1, GSTR 428; 2, Fielder; 3-10, T_0C734-1 to T_0C734-8, respectively.



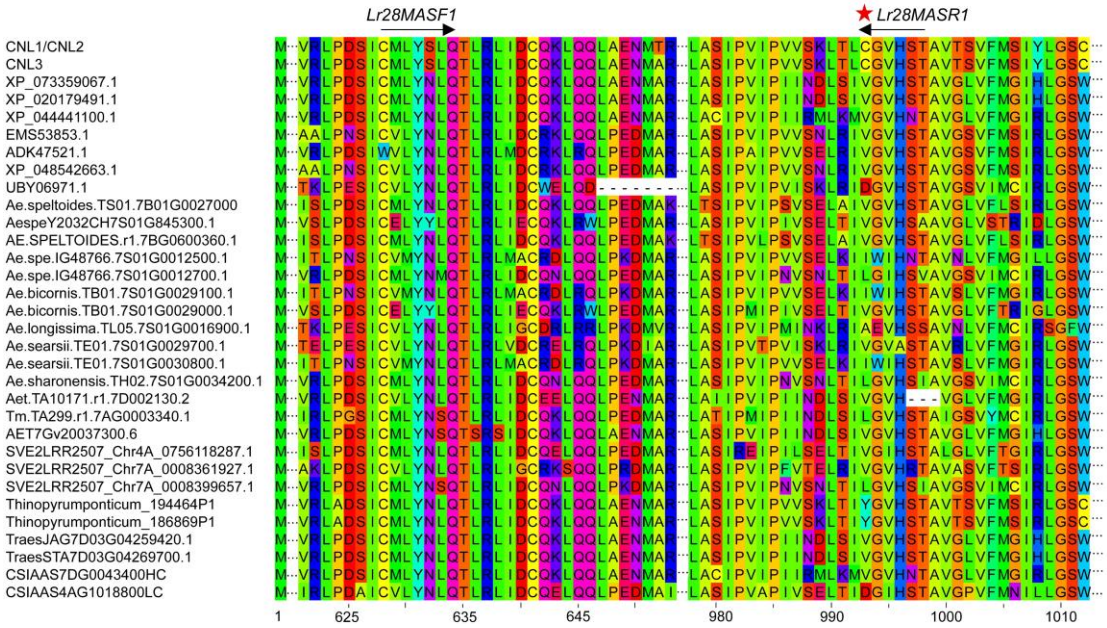
Supplementary Fig. 14. Characterization of T_0C749 (*CNL3*) transgenic complementation plants. a, PCR detection of the *CNL3* (gDNA) transgene using marker *Lr28F2R2* in T_0 transgenic plants. **b**, qRT-PCR analysis of *CNL3* expression. **c**, qRT-PCR amplification of *Actin* as an endogenous control. **d**, Disease reactions of GSTR 428, Fielder, and eight randomly selected T_0 transgenic plants following inoculation with *Pt* pathotype PHQS. R, resistant; S, susceptible. Lane designations: M, DNA marker; 1, GSTR 428; 2, Fielder; 3-10, T_0C749-1 to T_0C749-8, respectively.



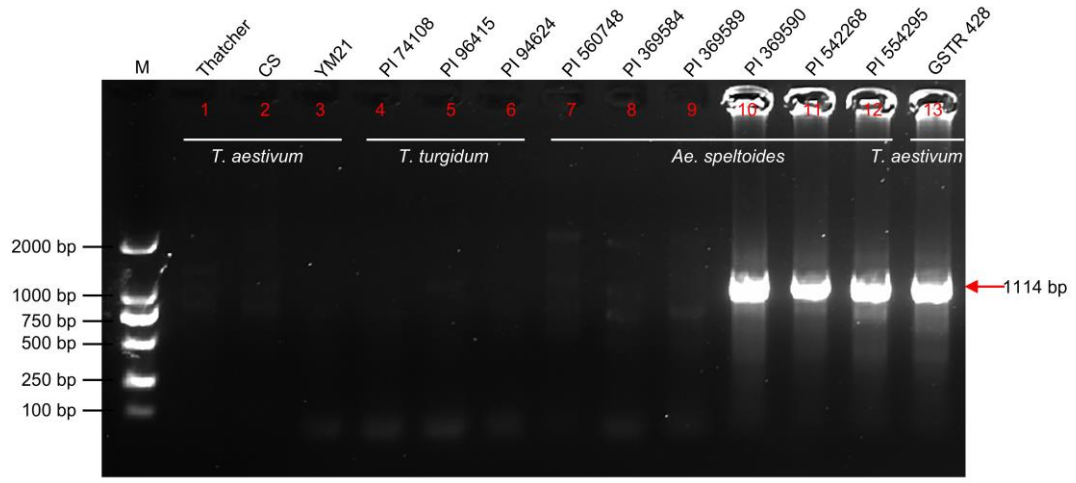
Supplementary Fig. 15. Phylogenetic tree of NLR proteins related to CNL1/CNL2 and CNL3. A neighbor-joining tree was constructed using CNL1/CNL2, CNL3, and their closest homologs from *Aegilops*, *Triticum*, other *Triticeae* species, and the NCBI non-redundant protein sequence database. Protein sequences were aligned with MUSCLE in MEGA7, and the tree was built using the neighbor-joining method with 1,000 bootstrap replicates. The tree was visualized with Interactive Tree Of Life (iTOL) v7 (https://itol.embl.de/). CNL1/CNL2 and CNL3 are highlighted in red.



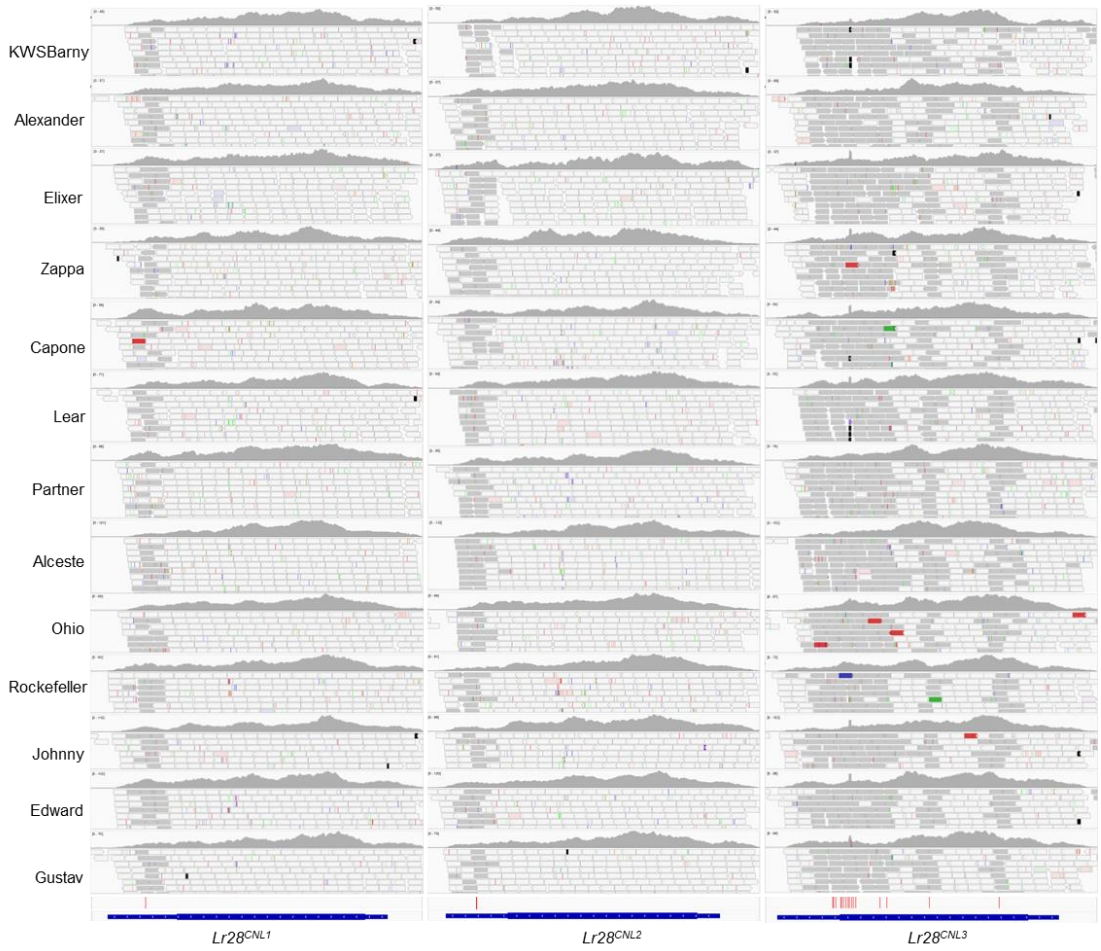
Supplementary Fig. 16. Phylogenetic analysis of CNL1/CNL2 and CNL3 with 207 known R proteins from Poaceae. Multiple sequence alignment was performed with MUSCLE in MEGA 7, and the tree was constructed using the Neighbor-Joining method with 1000 bootstrap replicates. The resulting tree was visualized using the Interactive Tree Of Life (iTOL) v7 (https://itol.embl.de/). CNL1/CNL2 and CNL3 are highlighted in red.



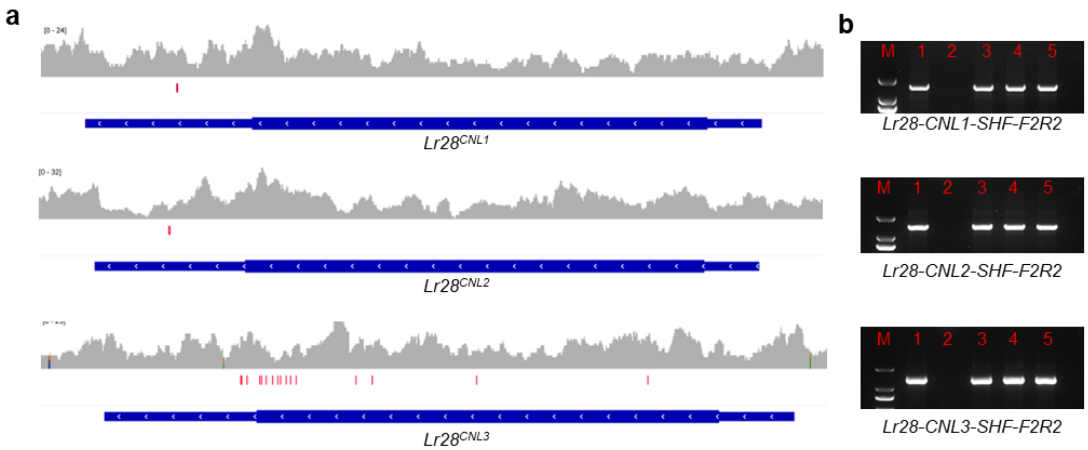
Supplementary Fig. 17. Location of the diagnostic marker *Lr28MASF1R1*. The critical polymorphism, amino acid 993C (marked with a red star), was used to develop the marker. Arrows indicate the primer binding sites and their orientation.



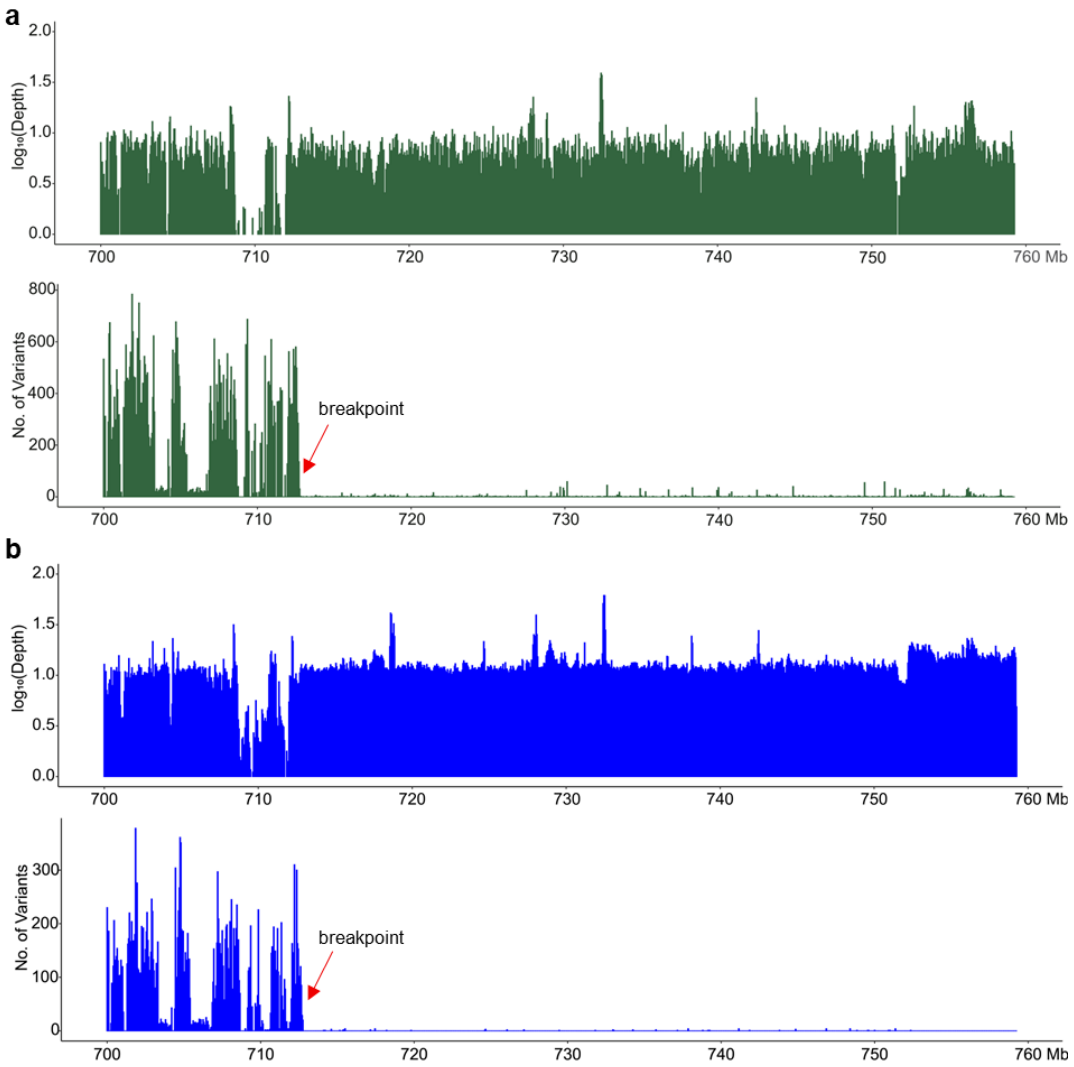
Supplementary Fig. 18. PCR amplification using the diagnostic marker *Lr28MASF1R1*. The expected 1114-bp amplicon (indicated by a red arrow) was detected in genotypes PI 369590, PI 542268, PI 554295, and GSTR 428 (lanes 10-13). No amplification was observed in *T. aestivum* lines Thatcher, CS, and YM21 (lanes 1-3), *T. turgidum* accessions PI 74108, PI 96415, and PI 94624 (lanes 4-6), or *Ae. speltoides* genotypes PI 560748, PI 369584, and PI 369589 (lanes 7-9). M, DNA marker.



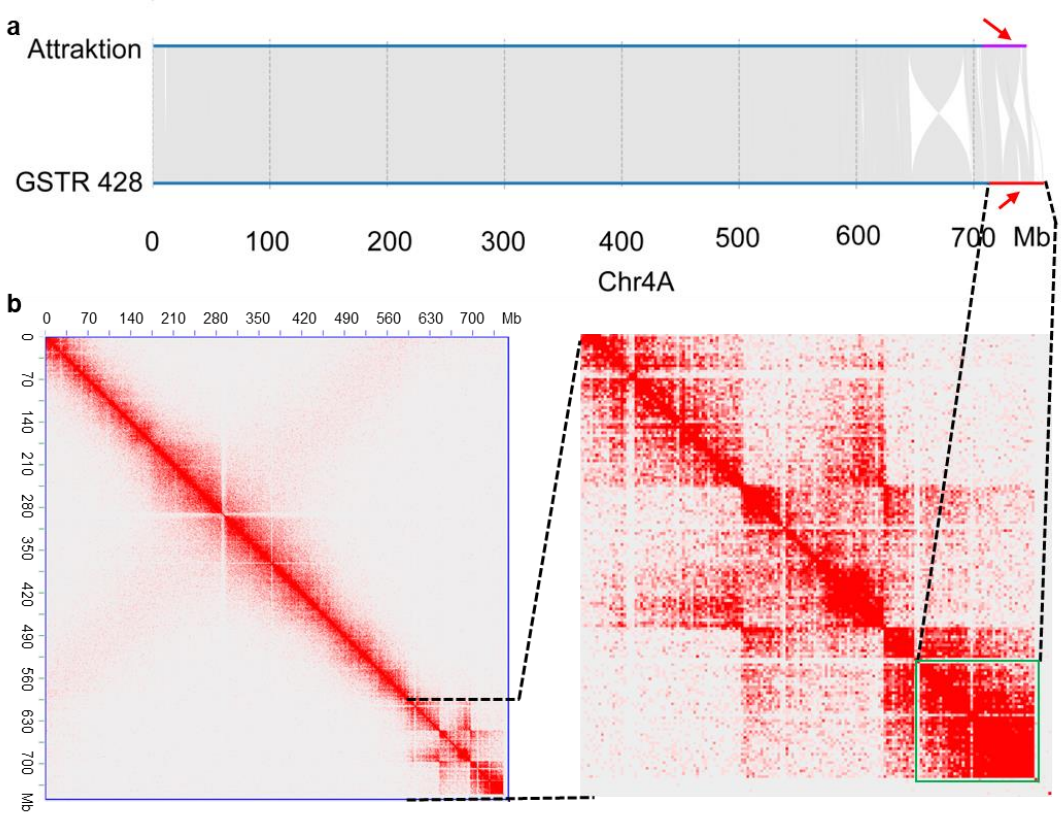
Supplementary Fig. 19. IGV snapshots showing RenSeq reads from 13 wheat cultivars aligned to *Lr28*^{CNL1}, *Lr28*^{CNL2}, and *Lr28*^{CNL3}. Coverage tracks indicate alignment depth at each nucleotide position. In the alignment panels, gray reads represent uniquely mapped reads and white reads denote multi-mapping reads. Red vertical lines at the bottom of the alignment panels indicate gene specific polymorphisms.



Supplementary Fig. 20. Analysis of the *Lr28* locus in the wheat cultivar Robigus. **a**, IGV snapshots showing whole-genome sequencing reads from Robigus aligned to the three *Lr28* genes. Red lines indicate gene-specific polymorphisms. **b**, PCR amplification using gene-specific markers for $Lr28^{CNL1}$ (top), $Lr28^{CNL2}$ (middle), and $Lr28^{CNL3}$ (bottom). The expected amplicons were detected in GSTR 428 (positive control) and Robigus, but not in Thatcher (negative control). Lane M: 2,000-bp DNA ladder; Lane 1: GSTR 428; Lane 2: Thatcher; Lanes 3-5: three independent Robigus samples.



Supplementary Fig. 21. Identification of the translocation breakpoints in Attraktion (a) and Robigus (b) using the GSTR 428 genome assembly. For each cultivar, the upper panel shows read depth coverage, and the lower panel shows the distribution of variants, both calculated in 50-kb sliding windows after aligning sequencing reads to the GSTR 428 genome. Red arrows mark the translocation breakpoints identified in each cultivar relative to the GSTR 428 reference.



Supplementary Fig. 22. Comparative sequence analysis of the distal 4AL region carrying *Lr28* in Attraktion and GSTR 428. a, Synteny analysis of chromosome 4A between Attraktion and GSTR 428. The introgressed alien segments are marked in purple in Attraktion and in red in GSTR 428 (indicated by red arrows). **b**, Hi-C interaction heatmaps. The left panel shows the interaction map of the entire chromosome 4A, and the right panel provides a magnified view of the distal 4AL region. The introgressed region is highlighted by a green box.